

# First-principles calculations of vibrational spectra of CdSe/CdS superlattices

A. I. Lebedev\*

*Physics Department, Moscow State University, 119991 Moscow, Russia*

(Dated: October 29, 2021)

The vibrational spectra of CdSe/CdS superlattices (SLs) with different layer thicknesses are calculated from first principles within the density functional theory. It is shown that, along with folded acoustic and confined optical modes, a number of confined acoustic modes appear in SLs. In structures with a minimum thickness of one of the layers, microscopic interface modes similar to local and gap modes in crystals appear. An analysis of projections of the eigenvectors of vibrational modes in SLs onto the orthonormal basis of normal modes in binary compounds enables to establish the details of formation of these vibrational modes and, in particular, to determine the degree of intermixing of acoustic and optical modes. A comparison of the frequencies of vibrational modes in CdSe/CdS SLs and CdSe/CdS nanoplatelets enables to separate the influence of size quantization and surface relaxation on the vibrational frequencies in the nanoplatelets.

DOI: 10.21883/FTT.2021.12.51663.156 (Physics of the Solid State (2021))

Keywords: phonon spectra, semiconductor superlattices, cadmium selenide, cadmium sulfide, nanostructures

## I. INTRODUCTION

Vibrational spectroscopy techniques—Raman scattering and infrared (IR) absorption—are powerful tools for analyzing the properties of various materials. These methods have found a wide application in studies of low-dimensional structures [1–3]. They provide information on the real structure of the samples under study: their composition, size, mechanical strains present in them, the state of the interfaces, and surface relaxation of atoms. However, the interpretation of the obtained results is often insufficiently substantiated. The aim of this work is to analyze the vibrational spectra of CdSe/CdS superlattices (SLs) in order to help in this interpretation. As a result of numerical modeling of the vibrational spectra of SLs, we will see a number of previously little discussed vibrational modes such as confined acoustic modes, gap modes, and local modes. In contrast to a large number of previous works, in which simplified models were usually used when calculating the lattice dynamics, in this work, we use the density functional theory approach, in which the electrical and mechanical boundary conditions upon relaxation of the structure (in our case, the lattice parameters of materials differ by 4%) are taken into account and satisfied automatically.

The vibrational spectra of superlattices are subjects of studies for more than 40 years [4–26]. Already in the first papers, the main distinctive features of vibrational spectra of SLs have been established: the appearance in them of folded acoustic modes [4–6, 10–14] and confined optical modes [8, 10–14].

The folded modes are longitudinal acoustic (LA) and transverse acoustic (TA) vibrations that propagate in both materials, experiencing weak reflections at the boundaries of two materials differing in their acoustic properties. The frequency of such vibrations in two mate-

rials of the superlattice is the same, but the wave vectors are different. The period of the superlattice determines new periodic boundary conditions for the emergence of standing waves, and the fact that the Brillouin minizone of the SL is several times smaller than the Brillouin zone of bulk materials results in a folding of this zone in the growth direction so that a number of points from the bulk of the Brillouin zones of the raw materials are projected to the  $\Gamma$  point of the folded zone. Thus, a whole set of new vibrational modes appear in the SL at the center of the Brillouin zone. The appearance of discontinuities in the energy spectrum of the modes (stop bands) observed at the center and at the boundary of the Brillouin minizone is associated with the difference in specific acoustic impedances of the used materials.

In the region of optical vibrations, confined modes, in which longitudinal optical (LO) and transverse optical (TO) vibrations are localized in one of two materials of the superlattice and are rapidly evanescent in another one, are observed. For such modes to appear, it is necessary that vibrations with a given frequency can propagate in one of the materials and cannot propagate in the other one. An indication of such vibrations is the absence of mode dispersion and the strong dependence of their frequency on the thickness of the layer of the first material.

Finally, under certain conditions, interface modes can arise in superlattices—modes localized at the interface between two materials, which are evanescent in both materials. Interface highly localized modes (they are also called *microscopic*) were first discovered in InAs/GaSb [27] and Ge/Si [28] superlattices. Like the confined modes, these modes are characterized by the absence of dispersion along the growth direction axis, but, in contrast to the confined modes, their frequencies remain unchanged with a change in the layer thickness. We note that the appearance of interface modes depends on the polarization of the vibrations: it is determined by how their frequencies relate to the frequencies in the continua formed by longitudinal and transverse modes in

---

\* swan@scon155.phys.msu.ru

bulk materials.

As follows from the experiment [9, 11–14], one more type of modes can arise in superlattices. They are also referred to as interface modes, although they are not strongly localized. These vibrational modes describe joint *macroscopic* vibrations of polar optical phonons in both materials of SL, in which the electric fields generated by them are coupled by electrostatic boundary conditions. In the limit of long waves, the frequencies of these modes satisfy the conditions  $d_1\epsilon_1(\omega) + d_2\epsilon_2(\omega) = 0$  or  $d_1\epsilon_2(\omega) + d_2\epsilon_1(\omega) = 0$ , where  $d_i$  is the thickness of the  $i$ th layer in the SL, and  $\epsilon_i$  is its complex dielectric constant [9, 29]. Since one of the dielectric constants must be negative to fulfill these conditions, these frequencies fall into the Reststrahlen band of one of the materials, that is, they lie between the frequencies of TO and LO phonons in this bulk material. These modes can be easily distinguished since their frequencies depend on the ratio of the layer thicknesses. To observe these modes, studies of Raman spectra are usually carried out *under resonance conditions* [9]. In contrast to the microscopic interface modes, in which atomic vibrations are localized at the interfaces, a much larger number of atoms usually participate in the vibrations of macroscopic interface modes (in the long-wave limit, all atoms in both layers [10, 30]).

The above results obtained for superlattices are also useful for understanding the vibrational spectra of other quasi-two-dimensional structures—nanoplatelets [31–33].

## II. CALCULATION TECHNIQUE

First-principles calculations were performed within the density functional theory in the plane-wave basis and the local density approximation (LDA) using the ABINIT software package [34]. Optimized pseudopotentials for Cd, S, and Se atoms were constructed according to the RRKJ scheme [35] using the *opium* program. The maximum energy of plane waves in the calculations was 30 Ha (816 eV). Integration over the Brillouin zone was carried out using the  $8 \times 8 \times 4$  or  $8 \times 8 \times 2$  Monkhorst–Pack meshes. The lattice parameters and equilibrium positions of atoms in superlattices oriented in the [001] direction and containing up to twelve monolayers of semiconductor were obtained from the condition that the Hellmann–Feynman forces become less than  $5 \cdot 10^{-6}$  Ha/Bohr (0.25 meV/Å) while the accuracy of calculating the total energy is better than  $10^{-10}$  Ha. The phonon spectra of the obtained equilibrium structures were calculated using the density-functional perturbation theory analogously to [36].

In this work, when determining the nature of vibrational modes, we will analyze the dispersion of these modes along the  $\Lambda$  axis of the Brillouin zone, since in real space it corresponds to the  $z$  direction in which strong perturbations are created in the superlattice structure. Fortunately, a high symmetry of the little group of the  $\Lambda$  wave vector retains the division of vibrations into the

longitudinal and transverse ones. We will not try to establish whether these modes belong to macroscopic interface modes since for this it is necessary to analyze their properties at nonzero transverse component of the phonon wave vector.

## III. CALCULATION RESULTS AND THEIR DISCUSSION

### A. Phonon spectra of superlattices

The symmetry of all superlattices studied in this work is described by the  $P\bar{4}m2$  space group, and the phonon modes at the  $\Gamma$  point can have the  $A_1$ ,  $B_2$ , and  $E$  symmetry. In Figs. 1 and 2 the eigenvectors of all optical modes for the  $(\text{CdSe})_6(\text{CdS})_6$  SL as well as their frequencies and symmetries are shown. As follows from the figures, all presented optical modes are confined: the vibrations are localized in one material of the SL and rapidly decay in the second material.

An analysis of the dispersion curves for optical modes (Fig. 3) shows that in the  $\Gamma$ – $Z$  direction the frequencies of these modes are practically independent of the wave vector (changes in the mode frequencies do not exceed  $0.01 \text{ cm}^{-1}$ ). This behavior is consistent with the existing concept of confined modes: they do not exhibit dispersion, but their frequencies depend on the thickness of the SL layers. The latter was demonstrated on  $(\text{CdSe})_n(\text{CdS})_n$  SLs with individual layer thicknesses of  $n = 1$ –4.

When discussing the behavior of dispersion curves in the Brillouin zone of a tetragonal structure, the following should be borne in mind. When moving from the  $\Gamma$  point to the  $\Lambda$  axis, the compatibility relations of irreducible representations describing the symmetry of normal vibrations are as follows:  $A_1 \rightarrow \Lambda_1$ ,  $B_2 \rightarrow \Lambda_1$ ,  $E \rightarrow \Lambda_3 + \Lambda_4$  ( $\Lambda_3$  and  $\Lambda_4$  are conjugate representations degenerate in frequency) [37]. Thus, on the  $\Lambda$  axis, only longitudinal  $A_1$  and  $B_2$  modes can mix with each other, although the mixing of acoustic and optical modes is also allowed. When moving from the  $\Gamma$  point along the  $\Delta$  and  $\Sigma$  axes of the Brillouin zone, the situation is different: the compatibility relations  $A_1 \rightarrow \Delta_1$ ,  $B_2 \rightarrow \Delta_1$ ,  $E \rightarrow \Delta_1 + \Delta_2$  and  $A_1 \rightarrow \Sigma_1$ ,  $B_2 \rightarrow \Sigma_2$ ,  $E \rightarrow \Sigma_1 + \Sigma_2$  allow mixing of longitudinal and transverse vibrations. In this case, significant dispersion appears on the dispersion curves, and the  $E$  modes are strongly split. The component of the  $E$  mode, which transforms according to the  $\Delta_2$  representation, does not mix with the  $A_1$  and  $B_2$  modes polarized in the  $z$  direction, and therefore its eigenvector describes only the displacements  $\mathbf{u} \perp \mathbf{q}$  in the  $xy$  plane. The  $\Delta_1$  mode as well as both  $\Sigma_1$  and  $\Sigma_2$  modes experience intermixing and exhibit a complex displacements pattern in all three directions.

An analysis of the dispersion curves along the  $\Lambda$  axis in the region of acoustic vibrations finds folded longitudinal and transverse acoustic modes (Fig. 3) and the appear-

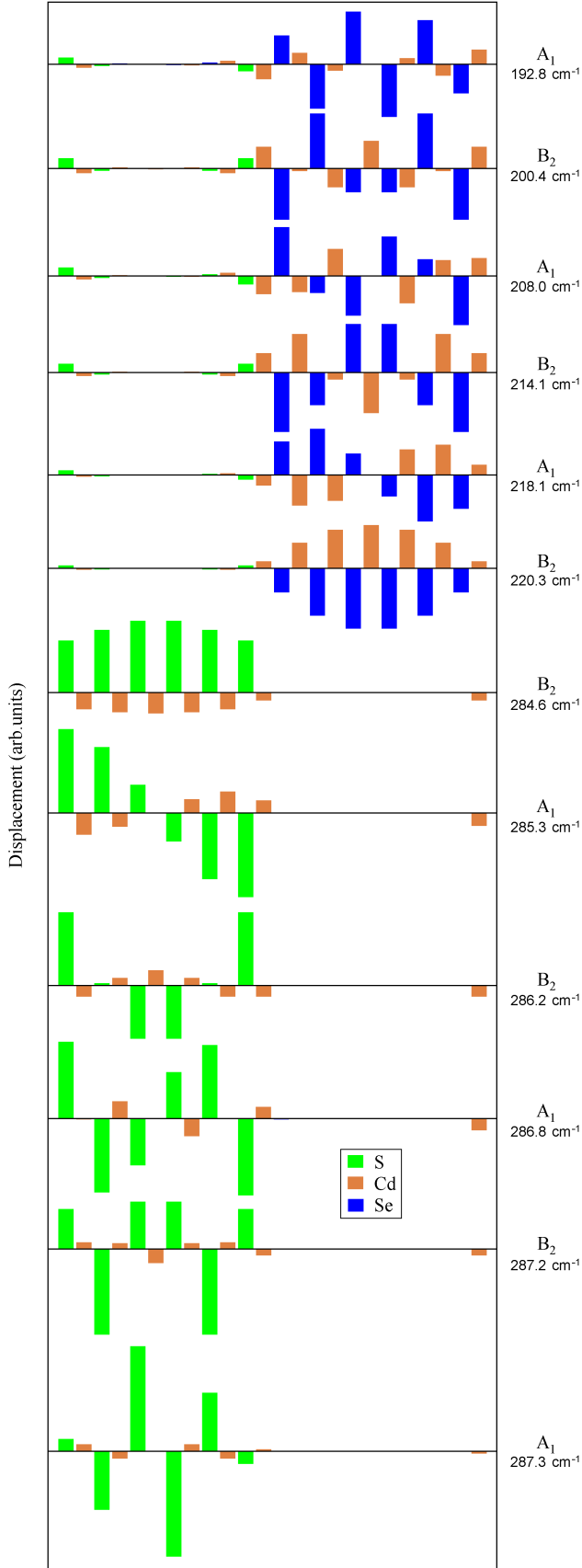


FIG. 1. Eigenvectors and frequencies of longitudinal optical modes with the  $A_1$  and  $B_2$  symmetry at  $\mathbf{q} \rightarrow 0$  in the  $(\text{CdSe})_6(\text{CdS})_6$  superlattice.

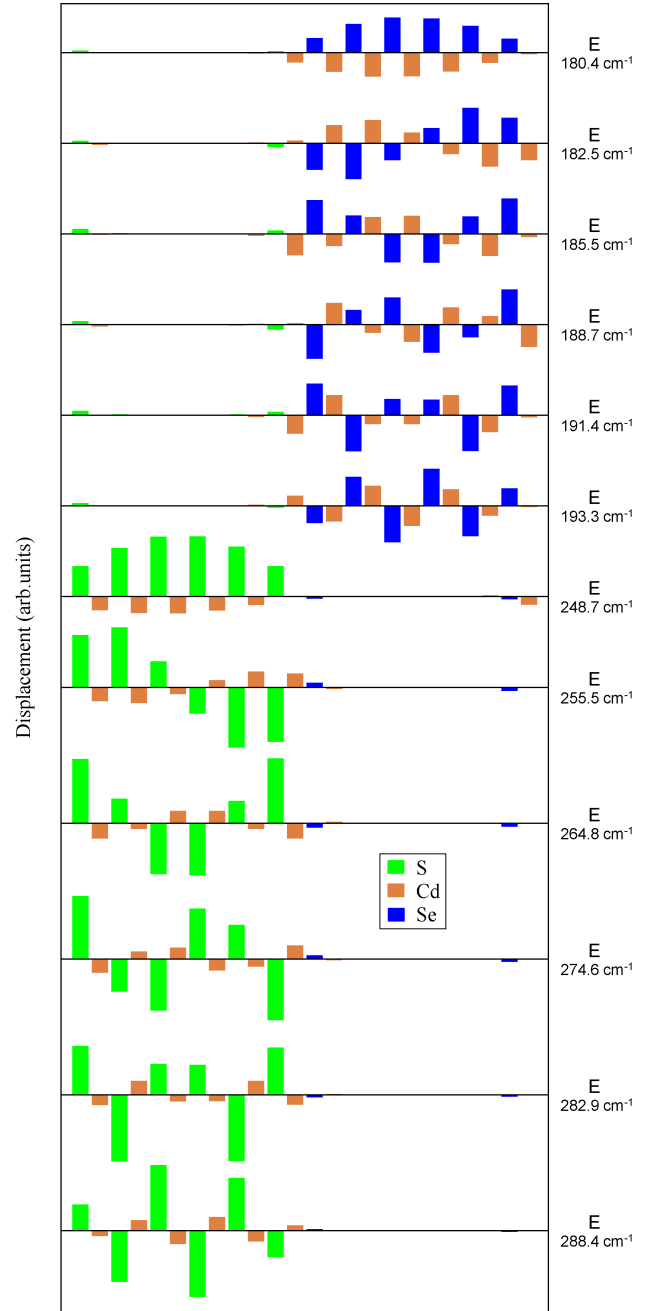


FIG. 2. Eigenvectors and frequencies of transverse optical modes of the  $E$  symmetry at  $\mathbf{q} = 0$  in the  $(\text{CdSe})_6(\text{CdS})_6$  superlattice.

ance, in the region of  $45\text{--}60\text{ cm}^{-1}$ , of several dispersionless TA modes, which will be discussed in Sec. III D.

Microscopic interface modes, whose eigenvectors are localized at the interface and which decay when moving into the interior of both materials, are not observed in CdSe/CdS SLs. Apparently, in superlattices whose materials have one common atom, this cannot be ob-

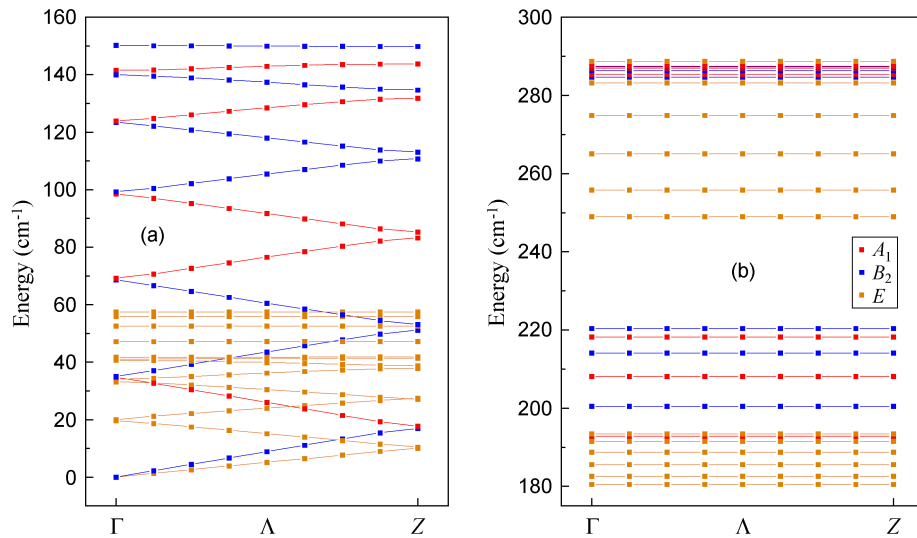


FIG. 3. Dispersion curves of (a) acoustic and (b) optical phonons in the  $(\text{CdSe})_6(\text{CdS})_6$  superlattice.

tained in principle because the frequencies of potential interface modes in these SLs fall into the continuum of optical vibrations of at least one of the materials of the SL. However, a kind of a microscopic interface mode can be created artificially if we consider the properties of SLs with extremely thin layers of one of the materials.

### B. Local and gap interface modes

The microscopic interface mode in a superlattice can be obtained from the confined mode when using the minimal thickness (one monolayer) of one of materials. If the frequency of this mode is outside the continuum of optical modes of the matrix, then such vibrations will not be able to propagate in the matrix and will be localized.

We performed a search for such modes in the  $(\text{CdSe})_{11}(\text{CdS})_1$  and  $(\text{CdSe})_1(\text{CdS})_{11}$  SLs, which contain one CdS monolayer in the CdSe matrix and one CdSe monolayer in the CdS matrix, respectively. As expected, localized optical modes of S and Se vibrations arised in the structures. In both cases, the incorporation of a monolayer into a matrix gives rise to three split-off modes whose symmetry ( $B_2 + E$ ) coincides with the symmetry of optical phonons in bulk materials ( $\Gamma_{15} \rightarrow B_2 + E$ ). In the CdSe matrix, the vibration frequencies of the S layer are, respectively, 265.2 and 274.6  $\text{cm}^{-1}$ ; they lie above the upper limit of the optical modes continuum of the matrix and are local modes (here we use a terminology used for classification of localized vibrations of impurities in crystals). In the CdS matrix, the vibrational frequencies of the Se layer are 187.3 and 217.0  $\text{cm}^{-1}$ , respectively; they lie in the gap between the optical and acoustic modes continua and are the gap modes. The eigenvectors of the local and gap modes are shown in Fig. 4. The admix-

ture of acoustic vibrations to the transverse local *optical* mode reaches 20% at the Z point, and that to the transverse gap mode reaches 45% at the Z point. In the local and gap longitudinal modes, the admixture of acoustic vibrations does not exceed 1%.

As expected for the local modes, the dispersion of both the  $E$  and  $B_2$  modes along the  $\Lambda$  axis in the  $(\text{CdSe})_{11}(\text{CdS})_1$  SL is absent. When the thickness of the CdSe layer is decreased from 11 to 7 monolayers, the mode frequencies exhibit a slight change (by 0.16 and 0.41  $\text{cm}^{-1}$ , respectively), which is entirely due to a small (by 0.2%) change in the in-plane lattice parameter of the SL. The gap modes are also dispersionless, and with a decrease in the number of CdS monolayers from 11 to 7 at a fixed lattice parameter, their frequencies change by no more than 0.002  $\text{cm}^{-1}$ .

While the local modes are well known, the gap modes have been studied in less detail. The possibility of their appearance turns out to be more problematic, since for this the frequencies of these modes must fall into the gap between the acoustic and optical modes continua for both materials of the SL. For transverse vibrations in CdSe/CdS SLs, the upper limit of the acoustic modes continuum lies in the region of 60  $\text{cm}^{-1}$ , and the gap under discussion is rather large. For longitudinal vibrations, the possibility of the appearance of a gap mode is determined by the maximum frequency of the LA mode at the X point in CdS, which is 152.2  $\text{cm}^{-1}$ . We note, however, that because of the orthogonality of longitudinal and transverse modes everywhere on the  $\Lambda$  axis, the possibility of observing transverse gap modes turns out to be wider. For example, the *transverse* In-Sb gap mode observed in the GaSb/InAs SLs in Ref. [27] remained dispersionless (i.e., localized) despite the fact that it was superimposed on the *longitudinal* optical modes contin-

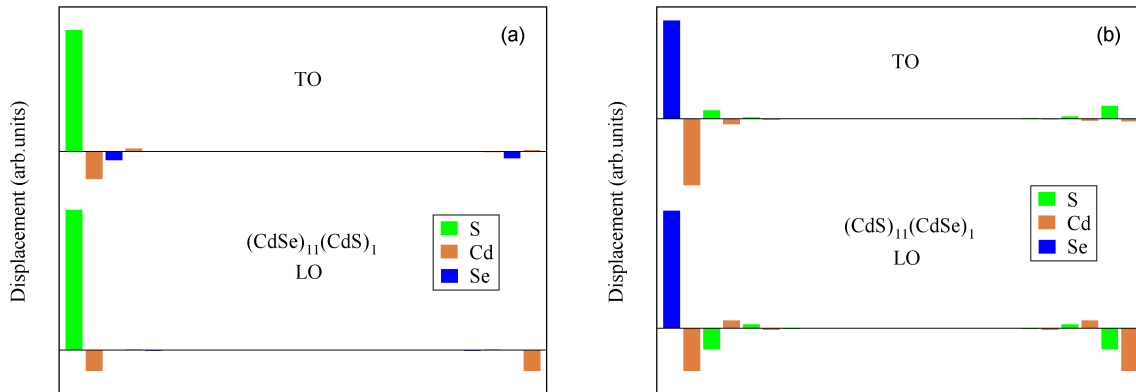


FIG. 4. Eigenvectors of the (a) local and (b) gap LO and TO modes at  $\mathbf{q} \rightarrow 0$  in  $(\text{CdSe})_{11}(\text{CdS})_1$  and  $(\text{CdSe})_1(\text{CdS})_{11}$  superlattices.

uum for one of materials of the SL (InAs).

Calculations show that the contributions of localized modes to the Raman and IR spectra are large enough to be observed experimentally.

### C. Dependence of TO-mode frequencies on the superlattice period

In Ref. [33], when studying the vibrational spectra of CdSe/CdS nanoplatelets, we discovered a mode associated with TO vibrations in the CdS layer, whose frequency rapidly decreased with increasing thickness of this layer. This mode gave the strongest contribution to the IR spectra from the CdS layers. The observed effect was explained by surface relaxation of the structure, which resulted in a noticeable shortening of the Cd–S interatomic distances near the surface and a corresponding increase in the vibrational frequency. The appearance of an  $E$  mode with similar properties in CdSe/CdS superlattices (lowest points in the upper block of frequencies in Fig. 5) and an analysis of the relaxations of the Cd–S distances (as compared to those in bulk CdS) when changing the period of  $(\text{CdSe})_n(\text{CdS})_n$  SLs showed that the maximum change in these distances in SLs is an order of magnitude smaller than in nanoplatelets, and moreover the changes in SLs have an opposite sign (Table I). This may mean that the mechanism proposed in [33] is not the only one.

In order to understand the origin of the strong effect of the thickness of CdS layer on the TO mode frequency in CdSe/CdS SLs, we analyzed the projections of the eigenvectors of vibrational modes in SLs by expanding them in the orthonormal basis of normal vibrations of LA, LO, TA, and TO phonons of bulk CdS with the zinc-blende structure,

$$\mathbf{Q}_\lambda^{\text{SL}} = \sum_{n=1}^4 \sum_q C_{nq}^\lambda \mathbf{Q}_{nq}^{\text{bulk}}, \quad (1)$$

TABLE I. Frequencies of TO modes giving the strongest contribution to the IR spectra from the CdS layers and the relaxation of the average Cd–S bond length for  $(\text{CdSe})_4/(\text{CdS})_n$  nanoplatelets and  $(\text{CdSe})_n(\text{CdS})_n$  superlattices with different number of monolayers  $n$  in the CdS layer. All calculations were performed using the same pseudopotentials.

$n$	Mode frequency ( $\text{cm}^{-1}$ )		Relaxation $R_{\text{Cd-S}}$	
	Nanoplatelet	Superlattice	Nanoplatelet	Superlattice
1	270.5	266.5	−0.758%	+0.522%
2	259.8	257.2	−0.248%	+0.485%
3	255.0	253.1	−0.114%	+0.478%
4	—	250.9	—	+0.473%
6	—	248.8	—	+0.470%

where  $\lambda$  is the number of the vibrational mode, and  $q$  is the wave vector of the normal mode. To make use of the orthogonality of normal modes, we should work with eigenvectors of the dynamical matrix  $\mathbf{Q}_{nq}$ , which are obtained by componentwise multiplication of the displacement vectors of the normal modes  $\mathbf{u}_{nq}$  by square roots of the masses of corresponding atoms.

The basis of the normal modes in bulk CdS was constructed according to a scheme similar to that used in Ref. [31]. First, the eigenvectors of LA, LO, TA, and TO phonons were calculated from first principles at 13 points of the Brillouin zone for dimensionless wave vectors  $0 \leq q_z \leq 1$  located between the  $\Gamma$  ( $q_z = 0$ ) and  $X$  ( $q_z = 1$ ) points of the Brillouin zone. The ratio of the displacements of Cd and S atoms for these phonons was approximated by a fourth-order polynomial of the  $\sqrt{\cos(\pi q_z/2)}$  function for longitudinal modes and the  $\cos^2(\pi q_z/2)$  function for transverse modes. These polynomials were then used to construct normalized basis functions for arbitrary value of  $q_z$ . For different  $q_z$ , the basis functions are orthogonal by construction. Check-

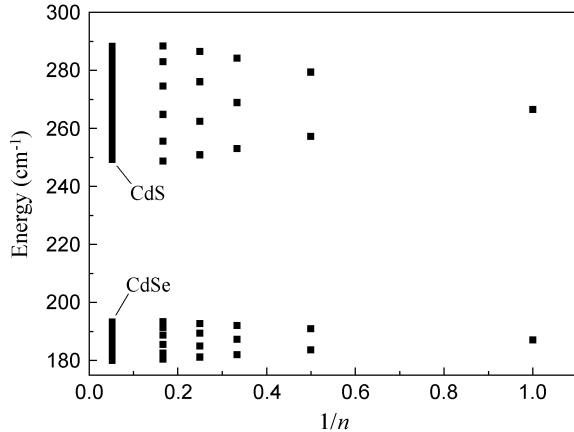


FIG. 5. Frequencies of TO modes at  $\mathbf{q} = 0$  in  $(\text{CdSe})_n(\text{CdS})_n$  superlattices. The wide vertical lines show the ranges of TO mode frequencies in CdSe and CdS binary compounds.

ing the basis functions for the same  $q_z$  showed that the deviation from their orthogonality does not exceed 0.003 for all  $q_z$  values.

The squared moduli of the  $C_{nq}^\lambda$  coefficients as a function of  $q_z$  for TO modes in SLs are shown in Fig. 6(a). The largest contribution to the displacement patterns of these modes is made by TO phonons of CdS; the contribution of TA phonons is about 100 times smaller. For the SL with the smallest thickness of the CdS layer, TO phonons from the entire Brillouin zone of bulk CdS contribute to this TO mode. Therefore, it is not surprising that the frequency of this mode in the  $(\text{CdSe})_1(\text{CdS})_1$  SL is close to the average frequency of TO vibrations in bulk CdS. With an increase in the thickness of the CdS layer, phonons from an increasingly narrow range of wave vectors in the vicinity of the  $\Gamma$  point start to dominate in the contributions, which, in accordance with the dispersion curve for TO phonons in bulk CdS, results in a decrease in the frequency of the optical mode.

The projection analysis of the displacement patterns for TO modes in  $(\text{CdSe})_4/(\text{CdS})_n$  nanoplatelets shows that the range of wave vectors contributing to these modes is noticeably narrower than in  $(\text{CdSe})_n(\text{CdS})_n$  superlattices with the same thickness of the CdS layer (Fig. 6). If the size quantization effect were the only one, the mode frequency in nanoplatelets would be lower than in superlattices. The fact that the opposite effect is actually observed (Table I) means that in nanoplatelets there exists one more contribution, namely the surface relaxation discussed in [33].

For the local TO mode in the  $(\text{CdSe})_{11}(\text{CdS})_1$  SL considered in Sec. III B, the projection onto TO phonons in CdS (Fig. 6(b)) is very similar to the projection for the  $(\text{CdSe})_1(\text{CdS})_1$  SL. However, in this case the contribution of TA modes becomes quite noticeable (21% in the vicinity of the  $X$  point). For the local LO mode in the  $(\text{CdSe})_{11}(\text{CdS})_1$  SL, the dominant contribution to this vi-

bration comes from LO phonons of CdS from the vicinity of the  $X$  point, but the fact that the frequency of this mode in the SL ( $274.6 \text{ cm}^{-1}$ ) is much lower than the frequency of LO phonon at the  $X$  point in CdS ( $300.6 \text{ cm}^{-1}$ ) may indicate a noticeable contribution of CdSe to this mode. The observed frequency shift is similar to the frequency shift for local vibrations of isolated impurities (for longitudinal local vibrations of the S impurity in the CdSe matrix, the calculated frequency is  $280.3 \text{ cm}^{-1}$ ).

#### D. Confined TA modes

In principle, the possibility of the appearance of confined TA modes arises from the difference in the spectra of acoustic vibrations in two materials of the superlattice. In particular, such modes were observed in GaSb/InAs SLs [27], where they were associated with the local vibrations of the Ga-As atomic pair located at the interface. The interface character of this mode was supported by the lack of dependence of its frequency on the thickness of layers in the superlattice. Similar modes did not appear at the In-Sb interface, since their frequencies fell into the continuum of acoustic modes of bulk materials.

An analysis of the acoustic modes in the phonon spectrum of the  $(\text{CdSe})_6(\text{CdS})_6$  SL finds in it, according to the vibration eigenvectors, four *confined* TA vibrational modes with frequencies of 47.9, 53.4, 56.8, and  $58.3 \text{ cm}^{-1}$  (Fig. 7). Similar modes were found in superlattices  $(\text{CdSe})_{11}(\text{CdS})_1$  (frequency  $52.0 \text{ cm}^{-1}$ ),  $(\text{CdSe})_{10}(\text{CdS})_2$  (frequencies 46.8 and  $56.6 \text{ cm}^{-1}$ ), and  $(\text{CdSe})_9(\text{CdS})_3$  (frequencies 51.7 and  $58.2 \text{ cm}^{-1}$ ). According to our estimates, the number of such modes in long-period SLs is about 70% of the number of CdS layers. Calculations of the dispersion curves along the  $\Lambda$  axis for these modes in  $(\text{CdSe})_6(\text{CdS})_6$  and  $(\text{CdSe})_{11}(\text{CdS})_1$  SLs show that the modes are dispersionless (the frequency change does not exceed  $0.01 \text{ cm}^{-1}$ , Fig. 3). Comparison of the frequencies of these modes with those of TA phonons at the  $X$  point in bulk crystals ( $45.0 \text{ cm}^{-1}$  in CdSe and  $55.0 \text{ cm}^{-1}$  in CdS) shows that transverse vibrations with such frequencies indeed cannot propagate in the CdSe layers and, therefore, are localized in the CdS layers. It is interesting that the frequencies of several of these modes even exceed the frequency of the upper limit of the acoustic continuum in bulk CdS. This may be due, first, to an admixture of up to 17–24% of optical vibrations to these acoustic modes, and second, to an increase in the frequency of TA phonons in the CdS layer upon biaxial stretching of the structure, which results from the addition of CdSe layers.

In SLs with a shorter period ( $(\text{CdSe})_4(\text{CdS})_4$ ), it is more difficult to draw conclusions about the nature of a mode from its eigenvector; however, the calculation of the mode dispersion along the  $\Lambda$  axis indicates that the mode with an energy of  $56.9 \text{ cm}^{-1}$  is dispersionless, and modes with frequencies of 53.1 and  $45.9 \text{ cm}^{-1}$  have a small dispersion ( $0.03$  and  $0.13 \text{ cm}^{-1}$ , respectively), which indi-

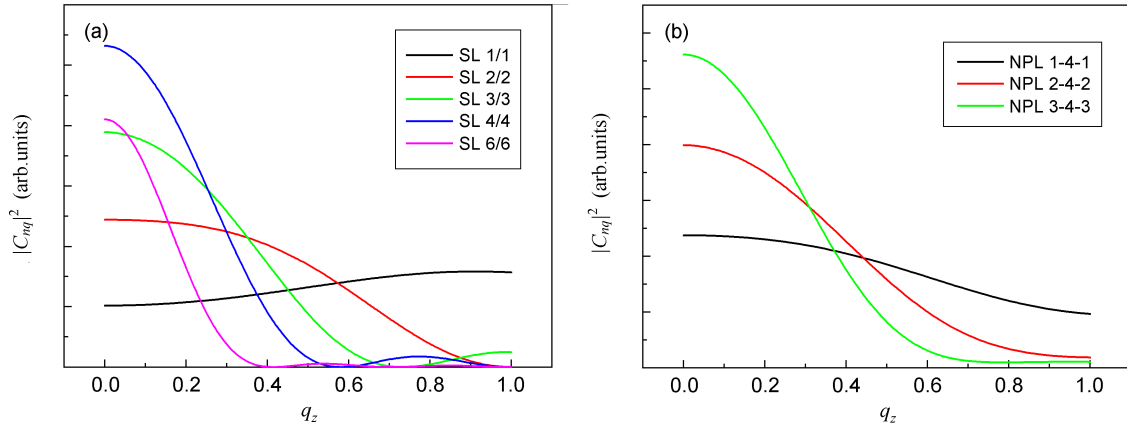


FIG. 6. Projections of the eigenvectors of TO modes giving the largest contribution to the IR spectra from the CdS layers onto the eigenvectors of TO phonons in bulk CdS with wave vectors between the  $\Gamma$  and  $X$  points for (a)  $(\text{CdSe})_n(\text{CdS})_n$  superlattices and (b)  $(\text{CdSe})_4/(\text{CdS})_n$  nanoplatelets.

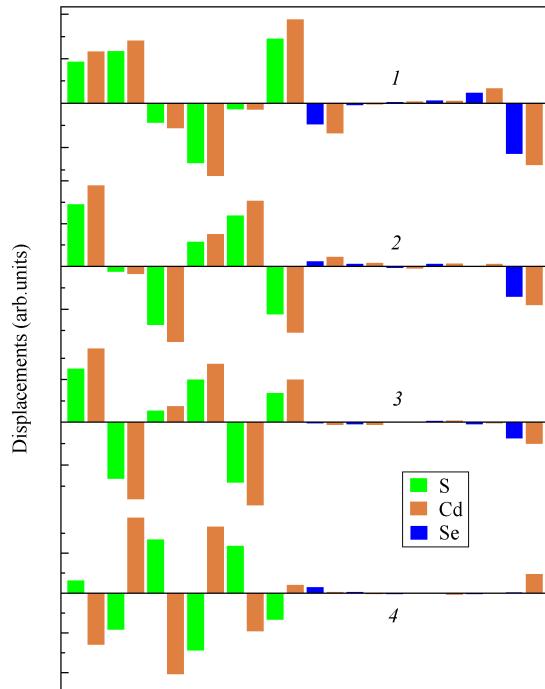


FIG. 7. Eigenvectors of four confined TA modes with frequencies of (1) 47.9, (2) 53.4, (3) 56.8, and (4) 58.3  $\text{cm}^{-1}$  ( $\mathbf{q} = 0$ ) in the  $(\text{CdSe})_6(\text{CdS})_6$  superlattice.

cates a weak interaction of vibrations in neighboring CdS layers in this SL (recall that the decay rate of vibrations increases when moving away from the upper limit of the acoustic modes continuum in the CdSe matrix, which is 45.0  $\text{cm}^{-1}$ ). Since the vibrational frequencies of the discussed TA modes depend on the layer thickness, these

modes are confined but not interface modes. Estimates of the contribution of the considered TA modes to the infrared and Raman spectra show that the experimental observation of these modes can be problematic, since their contribution to both types of spectra is rather small.

In continuation of our discussion on localized vibrations in SLs with one extremely thin layer, it is interesting to discuss whether the confined TA mode with a frequency of 52.0  $\text{cm}^{-1}$  arising in the  $(\text{CdSe})_{11}(\text{CdS})_1$  SL (Fig. 8) can be interpreted as an *interface mode*. In contrast to microscopic interface optical modes, the peculiarity of acoustic vibrations is that their eigenvectors have a double structure associated with the simultaneous occurrence of stretching and bending bond deformations that accompany lattice vibrations. The authors of Ref. [27] considered the TA mode with similar properties (resulting from the Ga-As pair vibrations in the GaSb/InAs SLs) as an interface mode. As in that work, the mode we are discussing is detached from the continuum of folded modes, is localized, and has no dispersion along the  $\Lambda$  axis. Very small (by 0.17  $\text{cm}^{-1}$ ) shift of the frequency of this mode when the thickness of the CdSe layer in the superlattice is decreased from 11 to 7 monolayers is entirely caused by a change in the in-plane lattice parameter of the SL and confirms the conclusion about its interface character. According to the projection analysis (Fig. 8(b)), the largest contribution to the discussed TA mode is given by TA phonons from a wide vicinity of the  $X$  point of bulk CdS with a noticeable (up to 30%) admixture of TO phonons (the same symmetry of these vibrations allows their mixing).

#### IV. CONCLUSIONS

In this work, the vibrational spectra of CdSe/CdS superlattices (SLs) are calculated from first principles

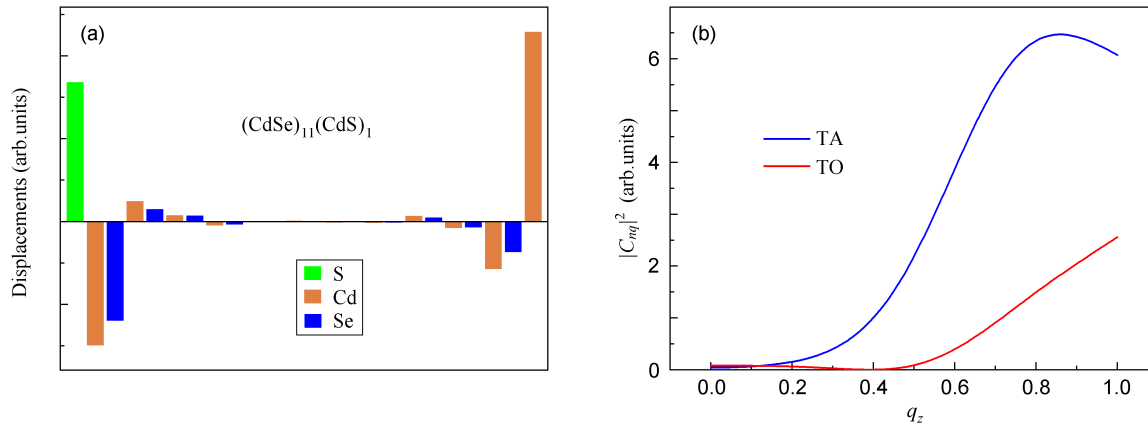


FIG. 8. (a) Eigenvector of the interface TA mode in the  $(\text{CdSe})_{11}(\text{CdS})_1$  superlattice. (b) Projections of the eigenvector of this mode onto the normal TA and TO modes of bulk CdS.

within the density functional theory. It is shown that along with folded acoustic and confined optical modes, a whole set of confined acoustic modes, whose number is  $\sim 70\%$  of the number of layers of material with a higher frequency of TA phonons, appears in the SLs. In structures with a minimum thickness of one of the layers, the formation of microscopic interface modes such as local

and gap modes is possible. An analysis of the projections of the eigenvectors of vibrational modes in SLs onto the orthonormal basis of normal modes in binary compounds finds a fairly intense mixing of acoustic and optical vibrations even in modes traditionally referred to as acoustic or optical.

- 
- [1] J.-P. Leburton, J. Pascual, and C. M. S. Torres, eds., *Phonons in Semiconductor Nanostructures* (Springer, Dordrecht, 1993).
- [2] P. Yu and M. Cardona, *Fundamentals of Semiconductors* (Springer-Verlag Berlin Heidelberg, 2010).
- [3] B. Jusserand and M. Cardona, Raman spectroscopy of vibrations in superlattices, in *Light Scattering in Solids. V* (Springer, Berlin, Heidelberg, 2006) Chap. 3, pp. 49–152.
- [4] J. L. Merz, A. S. Barker Jr., and A. C. Gossard, Raman scattering and zone-folding effects for alternating monolayers of GaAs–AlAs, *Appl. Phys. Lett.* **31**, 117 (1977).
- [5] A. S. Barker, J. L. Merz, and A. C. Gossard, Study of zone-folding effects on phonons in alternating monolayers of GaAs–AlAs, *Phys. Rev. B* **17**, 3181 (1978).
- [6] C. Colvard, R. Merlin, M. V. Klein, and A. C. Gossard, Observation of folded acoustic phonons in a semiconductor superlattice, *Phys. Rev. Lett.* **45**, 298 (1980).
- [7] F. Cerdeira, A. Pinczuk, J. C. Bean, B. Batlogg, and B. A. Wilson, Raman scattering from  $\text{Ge}_x\text{Si}_{1-x}/\text{Si}$  strained-layer superlattices, *Appl. Phys. Lett.* **45**, 1138 (1984).
- [8] A. K. Sood, J. Menéndez, M. Cardona, and K. Ploog, Resonance Raman scattering by confined LO and TO phonons in GaAs–AlAs superlattices, *Phys. Rev. Lett.* **54**, 2111 (1985).
- [9] A. K. Sood, J. Menéndez, M. Cardona, and K. Ploog, Interface vibrational modes in GaAs–AlAs superlattices, *Phys. Rev. Lett.* **54**, 2115 (1985).
- [10] C. Colvard, T. A. Gant, M. V. Klein, R. Merlin, R. Fischer, H. Morkoc, and A. C. Gossard, Folded acoustic and quantized optic phonons in  $(\text{GaAl})\text{As}$  superlattices, *Phys. Rev. B* **31**, 2080 (1985).
- [11] M. V. Klein, Phonons in semiconductor superlattices, *IEEE J. Quant. Electron.* **QE-22**, 1760 (1986).
- [12] J. Menéndez, Phonons in  $\text{GaAs-Al}_x\text{Ga}_{1-x}\text{As}$  superlattices, *J. Lumin.* **44**, 285 (1989).
- [13] M. Cardona, Folded, confined, interface, surface, and slab vibrational modes in semiconductor superlattices, *Superlattices Microstruct.* **5**, 27 (1989).
- [14] M. Cardona, Lattice vibrations in semiconductor superlattices, *Superlattices Microstruct.* **7**, 183 (1990).
- [15] V. A. Gaisler, A. O. Govorov, T. V. Kurochkina, N. T. Moshegov, S. I. Stenin, A. I. Toropov, and A. P. Shebanin, Phonon spectrum of GaAs–InAs superlattices, *JETP* **71**, 603 (1990).
- [16] G. Scamarcio, L. Tapfer, W. König, A. Fischer, K. Ploog, E. Molinari, S. Baroni, P. Giannozzi, and S. de Gironcoli, Infrared reflectivity by transverse-optical phonons in  $(\text{GaAs})_m/(\text{AlAs})_n$  ultrathin-layer superlattices, *Phys. Rev. B* **43**, 14754 (1991).
- [17] E. Molinari, S. Baroni, P. Giannozzi, and S. de Gironcoli, Effects of disorder on the Raman spectra of GaAs/AlAs superlattices, *Phys. Rev. B* **45**, 4280 (1992).
- [18] B. Samson, T. Dumelow, A. A. Hamilton, T. J. Parker, S. R. P. Smith, D. R. Tilley, C. T. Foxon, D. Hilton, and K. J. Moore, Effects of interface broadening on far-infrared and Raman spectra of GaAs/AlAs superlattices, *Phys. Rev. B* **46**, 2375 (1992).

- [19] J. Spitzer, T. Ruf, M. Cardona, W. Dondl, R. Schorer, G. Abstreiter, and E. E. Haller, Raman scattering by optical phonons in isotopic  $^{70}\text{Ge}_n^{74}\text{Ge}_n$  superlattices, *Phys. Rev. Lett.* **72**, 1565 (1994).
- [20] A. Yamamoto, T. Mishina, Y. Masumoto, and M. Nakayama, Coherent oscillation of zone-folded phonon modes in GaAs-AlAs superlattices, *Phys. Rev. Lett.* **73**, 740 (1994).
- [21] S. P. Kozyrev and L. K. Vodopyanov, Vibrational infrared spectroscopy of HgTe-CdTe superlattices, *Semicond. Sci. Technol.* **14**, 660 (1999).
- [22] A. G. Milekhin, A. I. Nikiforov, O. P. Pchelyakov, S. Schulze, and D. R. T. Zahn, Size-selective Raman scattering in self-assembled Ge/Si quantum dot superlattices, *Nanotechnology* **13**, 55 (2002).
- [23] R. R. Das, Y. I. Yuzyuk, P. Bhattacharya, V. Gupta, and R. S. Katiyar, Folded acoustic phonons and soft mode dynamics in BaTiO<sub>3</sub>/SrTiO<sub>3</sub> superlattices, *Phys. Rev. B* **69**, 132302 (2004).
- [24] A. V. Kosobutskii and E. N. Malysheva, Ab initio calculations of phonon spectra of (GaP)<sub>n</sub>(AlP)<sub>m</sub> superlattices, *Semiconductors* **42**, 1208 (2008).
- [25] Y. I. Yuzyuk, Raman scattering spectra of ceramics, films, and superlattices of ferroelectric perovskites: A review, *Phys. Solid State* **54**, 1026 (2012).
- [26] V. Davydov, E. Roginskii, Y. Kitaev, A. Smirnov, I. Elisseyev, D. Nechaev, V. Jmerik, and M. Smirnov, Phonons in short-period GaN/AlN superlattices: Group-theoretical analysis, ab initio calculations, and Raman spectra, *Nanomaterials* **11**, 286 (2021).
- [27] A. Fasolino, E. Molinari, and J. C. Maan, Calculated superlattice and interface phonons of InAs/GaSb superlattices, *Phys. Rev. B* **33**, 8889 (1986).
- [28] A. Fasolino and E. Molinari, Calculated phonon spectra of Si/Ge superlattices: analogies with other systems and new features, *J. Phys. Colloques* **48 Coll. C5**, 569 (1987).
- [29] R. Merlin, C. Colvard, M. V. Klein, H. Morkoç, A. Y. Cho, and A. C. Gossard, Raman scattering in superlattices: Anisotropy of polar phonons, *Appl. Phys. Lett.* **36**, 43 (1980).
- [30] R. E. Camley and D. L. Mills, Collective excitations of semi-infinite superlattice structures: Surface plasmons, bulk plasmons, and the electron-energy-loss spectrum, *Phys. Rev. B* **29**, 1695 (1984).
- [31] A. I. Lebedev, Lattice dynamics of quasi-two-dimensional CdSe nanoplatelets and their Raman and infrared spectra, *Phys. Rev. B* **96**, 184306 (2017).
- [32] S. V. Goupalov, Low-frequency vibrations of semiconductor nanoplatelets, *J. Phys. Chem. C* **123**, 11926 (2019).
- [33] A. I. Lebedev, B. M. Saidzhonov, K. A. Drozdov, A. A. Khomich, and R. B. Vasiliev, Raman and infrared studies of CdSe/CdS core/shell nanoplatelets, *J. Phys. Chem. C* **125**, 6758 (2021).
- [34] X. Gonze, B. Amadon, P.-M. Anglade, J.-M. Beuken, F. Bottin, P. Boulanger, F. Bruneval, D. Caliste, R. Caracas, M. Côté, T. Deutsch, L. Genovese, P. Ghosez, M. Giantomassi, S. Goedecker, D. R. Hamann, P. Hermet, F. Jollet, G. Jomard, S. Leroux, M. Mancini, S. Mazevet, M. J. T. Oliveira, G. Onida, Y. Pouillon, T. Rangel, G.-M. Rignanese, D. Sangalli, R. Shaltaf, M. Torrent, M. J. Verstraete, G. Zerah, and J. W. Zwanziger, Abinit: First-principles approach to material and nanosystem properties, *Computer Phys. Commun.* **180**, 2582 (2009).
- [35] A. M. Rappe, K. M. Rabe, E. Kaxiras, and J. D. Joannopoulos, Optimized pseudopotentials, *Phys. Rev. B* **41**, 1227 (1990).
- [36] A. I. Lebedev, Ab initio calculations of phonon spectra in ATiO<sub>3</sub> perovskite crystals ( $A = \text{Ca}, \text{Sr}, \text{Ba}, \text{Ra}, \text{Cd}, \text{Zn}, \text{Mg}, \text{Ge}, \text{Sn}, \text{Pb}$ ), *Phys. Solid State* **51**, 362 (2009).
- [37] Bilbao crystallographic server, <http://www.cryst.ehu.es/>.